Physics Letters B 770 (2017) 72–76

Contents lists available at ScienceDirect

Physics Letters B

www.elsevier.com/locate/physletb

Energy balance and deformation at scission in ^{240}Pu fission

Manuel Caamaño [a,*], Fanny Farget [b]

[a] Universidade de Santiago de Compostela, E-15706 Santiago de Compostela, Spain
[b] GANIL, CEA/DSM–CNRS/IN2P3, BP 55027, F-14076 Caen Cedex 5, France

ARTICLE INFO

Article history:
Received 22 December 2016
Received in revised form 3 March 2017
Accepted 20 April 2017
Available online 25 April 2017
Editor: D.F. Geesaman

Keywords:
240Pu fission
Inverse kinematics
Fragment deformation
Scission point

ABSTRACT

The experimental determination of the total excitation energy, the total kinetic energy, and the evaporation neutron multiplicity of fully identified fragments produced in transfer-induced fission of ^{240}Pu, combined with reasonable assumptions, permits to extract the intrinsic and collective excitation energy of the fragments as a function of their atomic number, along with their quadrupole deformation and their distance at scission. The results show that the deformation increases with the atomic number, Z, except for a local maximum around $Z = 44$ and a minimum around $Z = 50$, associated with the effect of deformed shells at $Z \sim 44$, $N \sim 64$, and spherical shells in ^{132}Sn, respectively. The distance between the fragments also shows a minimum around $Z_1 = 44$, $Z_2 = 50$, suggesting a mechanism that links the effect of structure with the length of the neck at scission.

1. Introduction

Soon after its discovery in 1939 [1,2], nuclear fission was understood as a long and complex process involving extreme deformations, nuclear structure, and heat flows that decide the characteristics of the emerging fission fragments distributions [3]. Among the many experimental observables, three of them helped to outline the current picture of the process: the fragment mass distribution revealed symmetric and asymmetric splits around favored fragment masses [4] that were soon related with the influence of nuclear shells [5,6]; the measurement of the total kinetic energy hinted at the magnitude of the fragment deformations and the existence of compact configurations centered on asymmetric splits [7]; the access to the multiplicity of neutrons evaporated by the fragments after scission contributed to better constrain the picture with hints on the amount of energy stored by each fragment at the end of the process [8,9]. These experimental observations led to a general interpretation where, in a very simplified picture, the fission proceeds according certain modes or channels around fragments with particular numbers of protons and/or neutrons, which emerge with specific deformations that also drive the sharing of part of the available energy [10,11].

Historically, the analysis of these experimental observables suffered from two main drawbacks: they are seldom obtained in the same experiment and the measurement of the fragment atomic number is either absent or scarce. The use of inverse kinematics in fission studies, pioneered by Schmidt et al. at GSI [12,13], opens a possibility to solve those issues. In particular, the access to the atomic number revealed that fragments were produced around certain proton numbers, instead of mass numbers, challenging the previous picture [14]. Currently, two complementary experimental campaigns take profit from the use of inverse kinematics: SOFIA at GSI, measuring electromagnetic-induced fission of neutron-deficient systems [15,16]; and the fission campaign in VAMOS/GANIL, where systems around ^{238}U are studied through transfer- and fusion-induced fission [17,18]. In this letter, we focus on the collection of observables measured in the VAMOS/GANIL experiments. These permit to extract the deformation and tip distance of the fragments at scission for ^{240}Pu through a detailed energy balance, as described in the following.

2. Energy balance at scission

The experimental information obtained in [17,21] used along this work includes the mass of the fissioning system, $M_{\rm FS}$, and its average excitation energy, $E^*_{\rm FS} = 9$ MeV, measured with the reconstruction of the ^{12}C(^{238}U, ^{240}Pu)^{10}Be transfer reaction producing ^{240}Pu fission [17]. Concerning the fission fragments, their masses after evaporation, $M_i^{\rm post}$, and before evaporation, M_i, deduced from their measured velocities [21], are also used. The information on the masses allowed the calculation of the neutron multiplicity, ν_i, the total kinetic energy at scission, *TKE*, and the total excitation energy, *TXE*, also in [21]. These fragment properties are expressed

* Corresponding author.
E-mail addresses: manuel.fresco@usc.es (M. Caamaño), farget@ganil.fr (F. Farget).

http://dx.doi.org/10.1016/j.physletb.2017.04.041

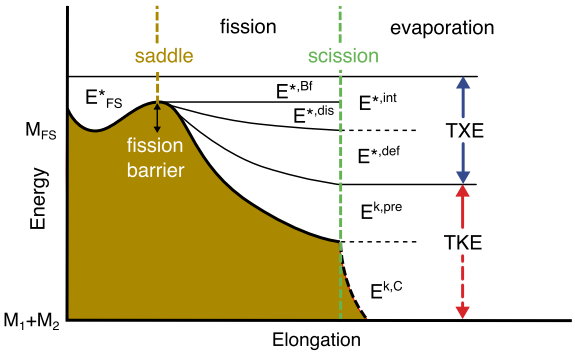

Fig. 1. Graphical explanation of the main components of the energy balance throughout the fission process. See text for details.

and used in this work as average values as a function of the fragment Z.

These data, combined with reasonable assumptions, permit to perform the energy balance of the process and deduce the excitation energy accumulated by the fragments as intrinsic and collective degrees of freedom. A first assumption considers that there is no evaporation of any kind from saddle to scission[1] and thus the total energy available in the fissioning system is stored in the nascent fragments at scission, in the form of excitation energy and kinetic energy for fully accelerated fragments (see Fig. 1 for reference):

$$E^*_{\mathrm{FS}} + M_{\mathrm{FS}} = M_1 + M_2 + TKE + TXE, \tag{1}$$

with the index 1 referring to any Z fragment and the index 2, to its partner with $Z_{\mathrm{FS}} - Z$.

TXE comprises the energy stored in each fragment from both collective and intrinsic degrees of freedom. The part of the energy corresponding to collective degrees of freedom, $E_i^{*,\mathrm{def}}$, is used in fragment deformation,[2] while intrinsic degrees of freedom are populated with the excitation energy available above the fission barrier, $E^{*,\mathrm{Bf}}$, and the energy dissipated by the fragments along the process, $E^{*,\mathrm{dis}}$:

$$TXE = E^{*,\mathrm{Bf}} + E^{*,\mathrm{dis}} + \sum_{i=1}^{2} E_i^{*,\mathrm{def}}. \tag{2}$$

The total excitation energy above the barrier, $E^{*,\mathrm{Bf}}$, is calculated with the subtraction of the fission barrier height from the excitation energy of the fissioning system, measured in the same experimental campaign [17,18], and resulting in an average of 3.3 MeV in the present case. The sum of the dissipated and deformation energy, $E^{*,\mathrm{dis}}$ and $E^{*,\mathrm{def}}$, corresponds to the remaining $TXE - E^{*,\mathrm{Bf}}$. Energetically, it is possible for $E^{*,\mathrm{dis}}$ to take values from 0 to $TXE - E^{*,\mathrm{Bf}}$, being *TXE* defined in Eq. (2). We can express this as:

$$E^{*,\mathrm{dis}} = F^{\mathrm{dis}} \left(TXE - E^{*,\mathrm{Bf}} \right), \tag{3}$$

with a factor F^{dis} that ranges from 0 to 1. The total intrinsic energy stored in the fragments, that is the sum $E^{*,\mathrm{Bf}} + E^{*,\mathrm{dis}}$, is reflected on the measurement of odd-Z fragments that result from the breaking of proton pairs in the descend from saddle to scission [23]. The amount of resulting intrinsic energy at scission can be related with the measured even–odd effect on the proton yields, δ_Z, defined as the difference between the cumulative yields of even- and odd-Z fragments. In Ref. [23], this relation is reported as $E^{*,\mathrm{Bf}} + E^{*,\mathrm{dis}} \sim -4\ln(\delta_Z)$, while in Refs. [24,25] is estimated that approximately 35% of the available $TXE - E^{*,\mathrm{Bf}}$ is transformed in $E^{*,\mathrm{dis}}$. Since both approaches give similar results in the present case, with $\delta_Z \sim 5\%$ [17],[3] we use the more general Eq. (3) with $F^{\mathrm{dis}} = 0.35$. Another source of pair breaking can be the dynamics of the neck rupture [26–28]. This source would reduce the value of F^{dis} when calculated only from the even–odd effect on fragment yields. In order to cover this situation, we shall also consider the extreme scenario of $F^{\mathrm{dis}} = 0$.

The intrinsic energy of each fragment, $E_i^{*,\mathrm{int}}$, results from the sharing of the total intrinsic energy available:

$$\sum_{i=1}^{2} E_i^{*,\mathrm{int}} = E^{*,\mathrm{Bf}} + E^{*,\mathrm{dis}}. \tag{4}$$

The partition of the total intrinsic energy between the fragments is calculated according to their level densities, described with the Gilbert–Cameron composite formula [30], following the prescription of Refs. [31,32].[4]

After scission, *TXE* is completely released by each fragment, in the form of neutron and γ emission:

$$TXE = \sum_{i=1}^{2} Q_i^n + \nu_i \varepsilon_i + E_i^{\gamma}, \tag{5}$$

with E_i^{γ} as the energy released in γ emission; the energy from neutron evaporation is the sum of the separation energy of the neutrons, Q_i^n, and their kinetic energy, expressed as an average energy, ε_i, multiplied by the measured neutron multiplicity, ν_i. Q_i^n is calculated with the masses at scission, M_i, and after evaporation, M_i^{post}, and with m_n, the neutron mass: $Q_i^n = M_i - \nu_i m_n - M_i^{\mathrm{post}}$. In average, the neutron evaporation competes with γ emission as long as the excitation energy of the fragment is higher than its neutron separation energy, Sn_i^{post}. For lower values, the fragment switches to only γ emission until the excitation energy is depleted [10]. Experimental results on low-energy fission of actinides show that the energy released in γ emission by each fragment is proportional to the neutron multiplicity, being the total energy similar to the neutron separation energy [33,34]. Following these experimental observations, we estimate E_i^{γ} from measured quantities as:

$$E_i^{\gamma} = Sn_i^{\mathrm{post}} \frac{\nu_i}{\nu_1 + \nu_2}. \tag{6}$$

Concerning the neutron average energy ε_i, it is found experimentally to evolve with the split but remains approximately equal for both fragments [35]. This behavior allows us to deduce ε for each split from Eq. (5), and to calculate the excitation energy for each fragment, E_i^*, as:

$$E_i^* = Q_i^n + \nu_i \varepsilon + E_i^{\gamma}. \tag{7}$$

[1] Scission neutron evaporation was estimated experimentally from 0 up to 30% of the total multiplicity [19], while state-of-the-art calculations for low-energy fission of ^{240}Pu report a value of ~ 0.6 neutrons, overall constant along the fragment mass [20]. The effect to our analysis is a slight shift of the absolute values while the general features and properties would remain. In order to reflect this effect, the error bars include said shift.

[2] The energy associated with other collective degrees, such as the angular momentum developed by the fragments, was estimated in values of the order of 1 MeV [22], and it is neglected in the present energy balance.

[3] With an average *TXE* between 29 to 30 MeV for the most produced splits, $E^{*,\mathrm{dis}}$ is of the order of 10 MeV, while from the even–odd effect we obtain $E^{*,\mathrm{dis}} \sim 9$ MeV.

[4] This prescription corresponds to the regime of statistical equilibrium, suitable for intrinsic excitation energies of the system of the order of $\sim$15 MeV [32], as in our case. In addition, the resulting energy partition is very similar when calculated following thermal equilibrium, suggesting that at this energy region, a complete sorting mechanism is very much reduced.

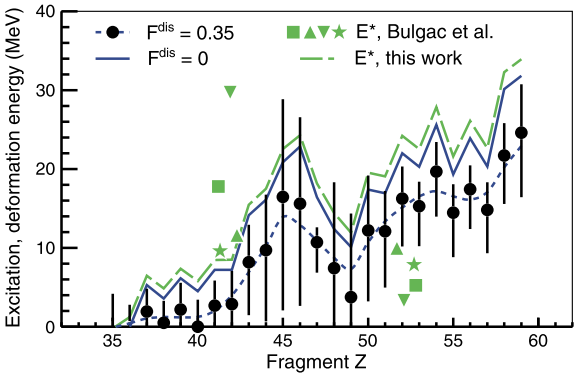

Fig. 2. (Color online) Deformation energy $E^{*,\mathrm{def}}$ as a function of the fragment Z for $F^{\mathrm{dis}} = 0.35$ (black dots). The short-dashed blue line is a moving average displayed as a guide to the eye. The solid blue line shows the upper limit of $E^{*,\mathrm{def}}$, set with $F^{\mathrm{dis}} = 0$. The long-dashed green line corresponds to the total excitation energy stored by the fragments, E^*, compared with the calculations of Bulgac et al. [29] (green symbols). The uncertainties on both lines are of the same order of those of the black dots.

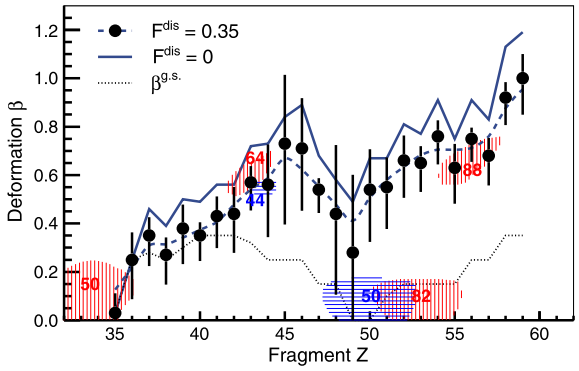

Fig. 3. (Color online) Deformation parameter β (dots). The solid blue line shows the maximum deformation allowed by energy conservation. The dashed blue line is a moving average displayed as a guide to the eye. The hatched areas correspond to maxima in neutron (vertical red hatching) and proton (horizontal blue hatching), deformed and spherical shell corrections lower than −2.5 MeV [5]; the red (blue) numbers correspond to the approximate neutron (proton) number of the shell. The dotted black line shows the average deformation of the fragments at the ground state.

The deformation energy is calculated from Eqs. (2) and (4) as the remaining excitation energy after subtracting the intrinsic excitation energy:

$$E_i^{*,\mathrm{def}} = E_i^* - E_i^{*,\mathrm{int}}. \tag{8}$$

Fig. 2 shows the calculated deformation energy for fragments of ^{240}Pu as a function of the fragment Z. The results are computed for two cases: $F^{\mathrm{dis}} = 0.35$, as recommended in [24,25], and $F^{\mathrm{dis}} = 0$, corresponding to an extreme case with no dissipation. In the same figure, the total excitation energy stored in each fragment is compared with recent calculations performed by Bulgac et al., where energy density functional is implemented in a real-time microscopic framework to calculate fission of ^{240}Pu with $E^*_{\mathrm{FS}} \sim 8$ MeV [29]. We can see what the authors interpret as a quasi-spherical slightly-excited heavy fragment around $Z = 52$ and a highly-deformed highly-excited light one around $Z = 42$. There is a fair discrepancy with our results: at $Z \sim 52$ we find deformed fragments excited up to 20 MeV, while at $Z \sim 42$ we have similarly deformed fragments (see Fig. 3) with a relatively low excitation energy of ~ 10 MeV.

Concerning the kinetic energy in Eq. (1), the measured *TKE* includes the energy gained by the Coulomb interaction between the fragments, $E^{\mathrm{k,C}}$, and the prescission kinetic energy, $E^{\mathrm{k,pre}}$, resulted from the displacement of the fragments on their descend from saddle to scission and from the nuclear interaction at the breaking of the system:

$$TKE = E^{\mathrm{k,C}}(Z_1, Z_2, \beta_1, \beta_2, d) + E^{\mathrm{k,pre}}. \tag{9}$$

The Coulomb energy is a function that depends on the atomic number, Z_i, and deformation, β_i, of each fragment, and on the distance between their surfaces, or tip distance, d. In this work, $E^{\mathrm{k,C}}$ is computed with the Cohen–Swiatecki formula [36] applied to the electric repulsion of the fragments as two ellipsoids separated by a distance d and aligned along their major axes[5]; each ellipsoid is homogeneously charged with $Z_i e$ and has a major radius of $r_0 A_i^{1/3}(1 + \sqrt{5/(4\pi)}\beta_i)$, with A_i as the average mass number of fragment i at scission. Concerning the prescission energy, calculations of the average $E^{\mathrm{k,pre}}$ for low-energy fission of ^{240}Pu, or similar systems, vary from some 20 MeV [38,39] to 10 MeV [5,26,10], to even zero due to the competition between the pre-scission movement and the nuclear attraction energy [40]. In our case, we use the results from Ivanyuk et al. [41], where $E^{\mathrm{k,pre}}$ is calculated as a function of the fragment A within the two-center shell model parameterization, resulting in values ranging from 20 MeV at $A \sim 140$ down to 5 MeV for the most asymmetric splits of ^{240}Pu.

3. Deformation and tip distance in fission fragments

As we discussed in the previous section, the deformation of the fragments links both *TKE* and *TXE* measurements: the energy needed to produce these deformations is a large part of *TXE*, while *TKE* is dominated by the Coulomb repulsion between the fragments, which depends on their deformations and the distance between them. In order to translate $E_i^{*,\mathrm{def}}$ into fragment deformation, we compute the increase in energy of the Weizsäcker liquid-drop mass-formula, B, for variations in the surface and Coulomb terms due to small quadrupole deformations, following the prescription of Swiatecki [42]. The fragment deformation corresponds to the one that results of adding $E_i^{*,\mathrm{def}}$ to the ground-state deformation calculated in [43] (dotted line in Fig. 3):

$$E_i^{*,\mathrm{def}} = B(A_i, Z_i, \beta_i) - B(A_i, Z_i, \beta_i^{\mathrm{g.s.}}). \tag{10}$$

Fig. 3 shows the resulting deformation β as a function of Z, calculated as explained in the previous section. The maximum β allowed by the energy balance, corresponding to $F^{\mathrm{dis}} = 0$, is also displayed for reference. In general, the behavior of β is very similar to that of the excitation energy of the fragments (Fig. 2) and also to the well-known saw-tooth behavior of the neutron multiplicity [44]: we see a steady increase from quasi-spherical light fragments to highly-deformed heavier ones, disturbed by an oscillation around the symmetry, with a minimum towards $Z \sim 50$. This behavior can be described with the influence of spherical and deformed shells, as put forward by Wilkins et al. [5]: Fig. 3 shows the regions with stronger proton- and neutron-shell corrections [5], displayed as vertical red (neutron) and horizontal blue (proton) hatched areas. We observe the fragment deformation to go through these regions related to deformed and spherical shell gaps [45,46], with the exception of the spherical configurations corresponding to $Z = 50$ and $N = 82$. Around this region, it is expected that ^{132}Sn microscopic shells act upon the heavy, $Z \sim 50$ fragment, producing an almost spherical shape. At the same time,

[5] Octupole deformation is expected to be small and to oscillate around a zero value, and thus neglected. For a recent calculation and discussion on ^{240}Pu, see [37].

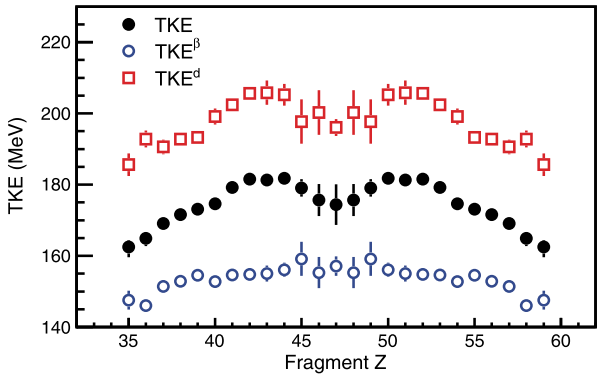

Fig. 4. (Color online) Contribution of the tip distance, TKE^{d} (empty red squares), and of fragment deformation, TKE^{β} (empty blue dots), to the measured *TKE* (black dots).

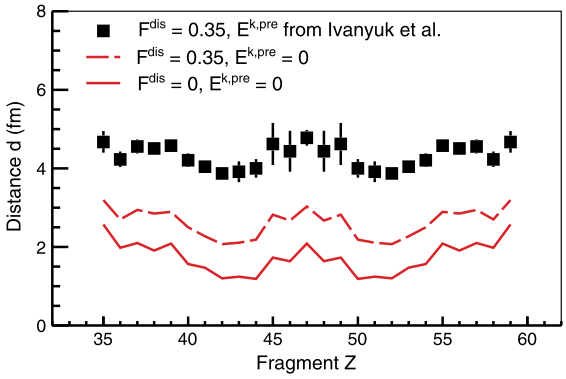

Fig. 5. (Color online) Distance between the surface of the fragments at scission, d, calculated with $F^{fis} = 0.35$ and $E^{k,pre}$ from Ref. [41] (squares), with $F^{dis} = 0.35$ and $E^{k,pre} = 0$ (dashed red line), and with $F^{dis} = 0$ and $E^{k,pre} = 0$ (solid red line).

this region is also affected by the macroscopic potential, which favors deformations of $\beta \sim 0.6$ [5]. The net effect of this competition appears as a shallow minimum in deformation, in between deformed and spherical shapes.[6] On the light-fragment side, the deformation of $Z \sim 44$ approaches two very close minima in proton and neutron shells for $\beta \sim 0.6$. These proton- and neutron-shell minima centered at $Z \sim 44$, $N \sim 64$, and those close to spherical ^{132}Sn seem to be responsible for the oscillation that forms the saw-tooth shape in β.

From the deduced β and the measured *TKE*, the tip distance between the fragments, d, can be extracted with Eq. (9), provided that we know the contribution of the prescission energy $E^{k,pre}$ to *TKE*. Fig. 5 shows the distance d in two scenarios: with $E^{k,pre}$ calculated as a function of the fragment Z by Ivanyuk et al. [41] and with $E^{k,pre} = 0$. It is noteworthy that only on this last case, d descends to values between 2 and 3 fm, around the "standard" distance for low-energy fission of actinides [5,10,47,14,48,25]. On a most realistic case with prescission energy, Fig. 5 shows the fragments separated between 4 and 5 fm, similar to the values used in recent scission-point models [49]. As a reference, the figure also shows a lower limit corresponding to no prescission energy and no dissipation, $E^{k,pre} = 0$ and $F^{dis} = 0$. In all the cases, Fig. 5 reveals a minimum for splits around $Z_1 = 44$, $Z_2 = 50$, where we also find deformed and spherical proton- and neutron-shells (see Fig. 3), suggesting a mechanism through which the formation of fragments around favored shells breaks the neck at a particular early stage, before it develops longer. Such mechanism might be related to the smaller probability of releasing nucleons from these shells, which remain preferably within the fragments, making the neck thinner and more brittle.

The minimum of d around $Z_1 = 44$, $Z_2 = 50$ also coincides with the maximum value of *TXE*, bringing the question whether is the distance and/or the deformation which shapes the behavior of the measured *TKE*. Fig. 4 shows the contributions of d and β, TKE^{d} and TKE^{β} respectively, to *TKE*. TKE^{d} is calculated as the Coulomb repulsion for spherical fragments at a distance d, while TKE^{β} corresponds to the interaction considering the deduced deformations and a fixed tip distance $d = 5$ fm. We can see that most of the features of *TKE* are governed by d. In particular, the observed maximum in TKE corresponds to a minimum in d, regardless of the deformation.

In summary, we showed the fragments deformation and tip distance at the scission point of low-energy ^{240}Pu fission deduced from experimental observables and few, reasonable assumptions. The results identify the influence of particular deformed and spherical shells, not only on the deformation but also on the tip distance. The present work with ^{240}Pu can also be considered as a first example of the new fission properties and observables made available by the recent generation of fission experiments with inverse kinematics. In the future, the same procedure is to be applied to other systems as a function of their excitation energy, giving an unprecedented insight on the evolution of the scission point with the initial conditions of the fission process.

[6] It is important to note that this shallow minimum is not a consequence of an underestimated value of F^{dis}. In order to approach deformations below $\beta < 0.1$, the dissipation would have to reach $F^{dis} \sim 0.6$, which is incompatible with the measured even–odd effect in one order of magnitude.

Acknowledgements

M.C. acknowledges the financial support of the Program "Ramón y Cajal" of the Ministerio de Economía y Competitividad of Spain through the grant number RYC-2012-11585. We thank B. Fernández Domínguez for her suggestions upon careful reading of the manuscript. We also thank the participants of the 2015 and 2016 fission workshops organized at GANIL (Caen) by FUSTIPEN for the fruitful discussions.

References

[1] O. Hahn, F. Strassmann, Über den Nachweis und das Verhalten der bei der Bestrahlung des Urans mittels Neutronen entstehenden Erdalkalimetalle, Naturwissenschaften 27 (1939) 11.
[2] L. Meitner, O. Frisch, Disintegration of uranium by neutrons: a new type of nuclear reaction, Nature 143 (1939) 239.
[3] N. Bohr, J.A. Wheeler, The mechanism of nuclear fission, Phys. Rev. 56 (1939) 426.
[4] K.F. Flynn, E.P. Horwitz, C.A.A. Bloomquist, R.F. Barnes, R.K. Sjoblom, P.R. Fields, L.E. Glendenin, Distribution of mass in the spontaneous fission of 256Fm, Phys. Rev. C 5 (1972) 1725, and references therein.
[5] B.D. Wilkins, E.P. Steinberg, R.R. Chasman, Scission-point model of nuclear fission based on deformed-shell effects, Phys. Rev. C 14 (1976) 1832.
[6] V.V. Pashkevich, On the asymmetric deformation of fissioning nuclei, Nucl. Phys. A 169 (1971) 275.
[7] H.C. Britt, H.E. Wegner, S.L. Whetstone, A comparison of fission fragment measurements made by double-energy and double-velocity techniques, Nucl. Instrum. Methods 24 (1963) 13, and references therein.
[8] H.R. Bowman, J.C.D. Milton, S.G. Thompson, W.J. Swiatecki, Further studies of the prompt neutrons from the spontaneous fission of 252Cf, Phys. Rev. 129 (1963) 2133.
[9] K.-H. Schmidt, B. Jurado, Entropy driven excitation energy sorting in superfluid fission dynamics, Phys. Rev. Lett. 104 (2010) 212501.
[10] U. Brosa, S. Grossman, A. Müller, Nuclear scission, Phys. Rep. 197 (1990) 167.
[11] M.G. Itkis, V.N. Okolovich, A.Ya. Rusanov, G.N. Smirenkin, Asymmetric fission of the pre-actinide nuclei, Z. Phys. A 320 (1985) 433.
[12] K.-H. Schmidt, A. Heinz, H.-G. Clerc, B. Blank, T. Brohm, S. Czajkowski, C. Donzaud, H. Geissel, E. Hanelt, H. Irnich, et al., Low-energy fission studies of neutron-deficient projectile fragments of 238U, Phys. Lett. B 325 (1994) 313.
[13] K.-H. Schmidt, S. Steinhäuser, C. Böckstiegel, A. Grewe, A. Heinz, A. Junghans, J. Benlliure, H.-G. Clerc, M. de Jong, J. Müller, M. Pfützner, B. Voss, Relativistic

radioactive beams: a new access to nuclear-fission studies, Nucl. Phys. A 665 (2000) 221.
[14] C. Böckstiegel, S. Steinhäuser, K.-H. Schmidt, H.-G. Clerc, A. Grewe, A. Heinz, M. de Jong, A.R. Junghans, J. Müller, B. Voss, Nuclear-fission studies with relativistic secondary beams: analysis of fission channels, Nucl. Phys. A 802 (2008) 12.
[15] T. Gorbinet, G. Bélier, G. Boutoux, A. Chatillon, A. Ebran, B. Laurent, J.-F. Martin, E. Pellereau, J. Taieb, L. Audouin, et al., A sample of the results of the first SOFIA experiment, Phys. Proc. 64 (2015) 101.
[16] J.-F. Martin, J. Taieb, A. Chatillon, G. Bélier, G. Boutoux, A. Ebran, T. Gorbinet, L. Grente, B. Laurent, E. Pellereau, et al., Studies on fission with ALADIN, Eur. Phys. J. A 51 (2015) 174.
[17] M. Caamaño, O. Delaune, F. Farget, X. Derkx, K.-H. Schmidt, L. Audouin, C.-O. Bacri, G. Barreau, J. Benlliure, E. Casarejos, et al., Isotopic yield distributions of transfer- and fusion-induced fission from 238U + 12C reactions in inverse kinematics, Phys. Rev. C 88 (2013) 024605.
[18] C. Rodríguez-Tajes, F. Farget, X. Derkx, M. Caamaño, O. Delaune, K.-H. Schmidt, E. Clément, A. Dijon, A. Heinz, T. Roger, et al., Transfer reactions in inverse kinematics: an experimental approach for fission investigations, Phys. Rev. C 89 (2014) 024614.
[19] N. Carjan, M. Rizea, Scission neutrons and other scission properties as function of mass asymmetry in 235U(nth,f), Phys. Rev. C 82 (2010) 014617, and references therein.
[20] R. Capote, N. Carjan, S. Chiba, Scission neutrons for U, Pu, Cm, and Cf isotopes: relative multiplicities calculated in the sudden limit, Phys. Rev. C 93 (2016) 024609, and references therein.
[21] M. Caamaño, F. Farget, O. Delaune, K.-H. Schmidt, C. Schmitt, L. Audouin, C.-O. Bacri, J. Benlliure, E. Casarejos, X. Derkx, et al., Characterization of the scission point from fission-fragment velocities, Phys. Rev. C 92 (2015) 034606.
[22] G.M. Ter-Akopian, J.H. Hamilton, Y.T. Oganessian, A.V. Daniel, J. Kormicki, A.V. Ramayya, G.S. Popeko, B.R.S. Babu, Q.-H. Lu, K. Butler-Moore, et al., Yields of correlated fragment pairs in spontaneous fission of 252Cf, Phys. Rev. C 55 (1997) 1146.
[23] F. Gönnenwein, The Nuclear Fission Process, CRC Press, London, 1991, p. 409.
[24] F. Rejmund, A.V. Ignatyuk, A.R. Junghans, K.-H. Schmidt, Pair breaking and even–odd structure in fission-fragment yields, Nucl. Phys. A 678 (2000) 215.
[25] K.-H. Schmidt, B. Jurado, C. Amouroux, C. Schmitt, General description of fission observables: GEF model code, Nucl. Data Sheets 131 (2016) 107.
[26] M. Asghar, R.W. Hasse, Saddle-to-scission landscape in fission: experiments and theories, J. Phys. (Paris) 45 (1984) C6-455.
[27] J.P. Bocquet, R. Brissot, Mass, energy and nuclear charge distributions of fission fragments, Nucl. Phys. A 502 (1989) 213c.
[28] B. Bouzid, M. Asghar, M. Djebara, M. Medkour, The nature of dynamics of the last stages of the fission process, J. Phys. G 24 (1998) 1029.
[29] A. Bulgac, P. Magierski, K.J. Roche, I. Stetcu, Induced fission of 240Pu within a real-time microscopic framework, Phys. Rev. Lett. 116 (2016) 122504.
[30] A. Gilbert, A.G.W. Cameron, A composite nuclear-level density with shell corrections, Can. J. Phys. 43 (1965) 1446.
[31] R. Capote, M. Herman, P. Obložinský, P.G. Young, S. Goriely, T. Belgya, A.V. Ignatyuk, A.J. Koning, S. Hilaire, V.A. Plujko, et al., RIPL – Reference Input Parameter Library for calculation of nuclear reactions and nuclear data evaluations, Nucl. Data Sheets 110 (2009) 3107.
[32] K.-H. Schmidt, B. Jurado, Final excitation energy of fission fragments, Phys. Rev. C 83 (2011) 061601(R).
[33] R. Vogt, J. Randrup, Event-by-event study of photon observables in spontaneous and thermal fission, Phys. Rev. C 87 (2013) 044602, and references therein.
[34] R. Capote, Y.-J. Chen, F.-J. Hambsch, N.V. Kornilov, J.P. Lestone, O. Litaize, B. Morillon, D. Neudecker, S. Oberstedt, T. Ohsawa, et al., Prompt fission neutron spectra of actinides, Nucl. Data Sheets 131 (2016) 1, and references therein.
[35] K. Nishio, Y. Nakagome, H. Yamamoto, I. Kimura, Multiplicity and energy of neutrons from 235U(nth,f) fission fragments, Nucl. Phys. A 632 (1998) 540.
[36] S. Cohen, W.J. Swiatecki, The deformation energy of a charged drop. IV. Evidence for a discontinuity in the conventional family of saddle point shapes, Ann. Phys. 19 (1962) 67.
[37] P. Goddard, P. Stevenson, A. Rios, Fission dynamics within time-dependent Hartree–Fock: deformation-induced fission, Phys. Rev. C 92 (2015) 054610.
[38] K.T.R. Davies, R.A. Managan, J.R. Nix, A.J. Sierk, Rupture of the neck in nuclear fission, Phys. Rev. C 16 (1977) 1890.
[39] L. Bonneau, P. Quentin, I.N. Mikhailov, Scission configurations and their implication in fission-fragment angular momenta, Phys. Rev. C 75 (2007) 064313.
[40] M.V. Borunov, P.N. Nadtochy, G.D. Adeev, Nuclear scission and fission-fragment kinetic-energy distribution: study within three-dimensional Langevin dynamics, Nucl. Phys. A 799 (2008) 56.
[41] F.A. Ivanyuk, S. Chiba, Y. Aritomo, Scission-point configuration within the two-center shell model shape parameterization, Phys. Rev. C 90 (2014) 054607.
[42] W.J. Swiatecki, Deformation energy of a charged drop. II. Symmetric saddle point shapes, Phys. Rev. 104 (1956) 993.
[43] J.-P. Delaroche, M. Girod, J. Libert, H. Goutte, S. Hilaire, S. Péru, N. Pillet, G.F. Bertsch, Structure of even–even nuclei using a mapped collective Hamiltonian and the D1S Gogny interaction, Phys. Rev. C 81 (2010) 014303.
[44] J.S. Fraser, J.C.D. Milton, Distribution of prompt-neutron emission probability for the fission fragments of 233U, Phys. Rev. 93 (1954) 818.
[45] V.M. Strutinski, Shell effects in nuclear masses and deformation energies, Nucl. Phys. A 95 (1967) 420.
[46] V.M. Strutinski, “Shells” in deformed nuclei, Nucl. Phys. A 122 (1968) 1.
[47] T.-S. Fan, J.-M. Hu, S.-L. Bat, Study of multichannel theory for the neutron induced fissions of actinide nuclei, Nucl. Phys. A 591 (1995) 161.
[48] H. Goutte, J.F. Berger, P. Casoli, D. Gogny, Microscopic approach of fission dynamics applied to fragment kinetic energy and mass distributions in 238U, Phys. Rev. C 71 (2005) 024316.
[49] J.-F. Lemaître, S. Panebianco, J.-L. Sida, S. Hilaire, S. Heinrich, New statistical scission-point model to predict fission fragment observables, Phys. Rev. C 92 (2015) 034617.